

We are IntechOpen, the world's leading publisher of Open Access books Built by scientists, for scientists

4,800

Open access books available

122,000

International authors and editors

135M

Downloads

Our authors are among the

154

Countries delivered to

TOP 1%

most cited scientists

12.2%

Contributors from top 500 universities



WEB OF SCIENCE™

Selection of our books indexed in the Book Citation Index
in Web of Science™ Core Collection (BKCI)

Interested in publishing with us?
Contact book.department@intechopen.com

Numbers displayed above are based on latest data collected.
For more information visit www.intechopen.com



Corneal Microlayer Optical Tomography Review

Vatookarn Roongpoovapatr, Jane C. Cook, Taher K. Eleiwa, Sonia H. Yoo and Mohamed Abou Shousha

Abstract

Anterior segment ultra-high resolution OCT (UHR-OCT) uses a resolution of 1–4 μm to provide non-invasive imaging of the tear film and cornea. This new high definition imaging technology increases our understanding of normal structure and pathological changes in the cornea, and resolution has continued to improve over time. UHR-OCT is useful in the treatment of disease such as dry eye, subclinical keratoconus, keratoconus, and ocular surface pathology. It also aids clinicians in fitting contact lenses and screening tissue for corneal transplantation. In this review, we summarize applications of imaging the normal and pathologic ocular surface and cornea. Novel developments, such as the new-generation micro-OCT, Anterior segment OCT angiography and artificial intelligence have the potential to continue to increase our knowledge.

Keywords: optical coherence tomography, optical biopsy, corneal microlayer, graft rejection, corneal imaging

1. Introduction

Speed and image quality of Optical Coherence Tomography (OCT) technology have made great strides over the past few decades [1–3]. OCT has long been a critical part of imaging the posterior segment, but is now starting to become more helpful for the anterior segment as well [3].

As anterior segment OCT has evolved, the precision of axial resolution has increased, from 15 to 20 μm resolution of time domain (TD-OCT) to 4–7 μm of spectral domain (SD-OCT) and Fourier-domain OCT (FD-OCT) and 1–4 μm of Ultra- high resolution OCT (UHR-OCT) [4, 5]. Speed has improved and UHR-OCT allows for real-time imaging and minimizes motion artifacts compared with older models [6–8]. Scan width of UHR-OCT has also improved to the current 5–12 mm [2–9].

This high definition imaging shows the *in vivo* pathological changes in microlayers of the cornea. Many publications have described the utility of UHR-OCT in clinical diagnosis and management of corneal disease [2, 10–13]. In the following review, we summarize the clinical applications of imaging the ocular surface and cornea based on anatomical structure and will focus on UHR-OCT.

2. Ultra-high resolution OCT

2.1 Technical aspects

Optical coherence tomography (OCT) is a non-contact image acquisition technology first developed by Huang et al. [14]. It produces an 'optical biopsy': detailed cross-sectional images of biological tissue [14]. Signal acquisition and processing methods determine image speed and resolution [15]. As resolution and tissue penetrance have improved, clinical applications continue to evolve [16].

The time-domain OCT (TD-OCT) was the first available anterior segment OCT, with the prototypes Visante and SL-OCT (Heidelberg Engineering, Heidelberg, Germany). Both acquired 2000 A-scans per second and had a resolution of 10–18 μm . These earlier models could scan the entire anterior segment, but were slow with poor resolution [1, 2]. Resolution improved to 5 μm with the SD-OCT, but scan width was limited at 3–6 mm. Available SD-OCTs included the Cirrus (Carl Zeiss Meditec, Inc.), Spectralis (Heidelberg Engineering, Dossenheim, Germany), RTVue (Optovue, Meridianville, AL), 3D OCT (Topcon Medical Systems, Oakland, NJ), and Bioptigen SD-OCT (Bioptigen Inc., Research Triangle Park, NC) [1, 2]. Swept-source (SS) Fourier-domain (FD) OCT was available in 2008 and the prototype was Casia SS OCT (Tomey, Nagoya, Japan). This SS-OCT had a scan width of 16 mm, depth of 6 mm and A-scan rate of 30,000 per second which then allowed for three-dimensional scanning of the entire anterior segment [1].

The first use of UHR-OCT was reported by Drexler et al. in 2001 with 2–3 resolution imaging of Bowman's membrane [17]. Current axial resolution of the UHR-OCT is 1–4 μm with a scan width of 5–12 mm [9, 10, 18]. OCT resolution was improved with a light source with a broad bandwidth greater than 100 nm and a specifically designed spectrometer which detected fringes collected from both reference and sample arms [2]. These changes allowed for *in vivo* imaging of individual corneal layers (microlayer), the tear film, tear meniscus and contact lens interfaces [9, 18, 19].

Most published data using UHR-OCT was acquired from custom-built machines, and availability. The Bioptigen Envisu (Bioptigen Inc., Research Triangle Park, NC, USA) and the SOCT Copernicus HR (Optopol Technologies SA, Zawiercie, Poland) are current commercially available models of UHR-OCT.

2.2 Corneal anatomy

The cornea is the transparent structure which, along with the tear film, provides about two-thirds of the refractive power of the eye [20]. The central cornea on average is 551–565 μm thick and the peripheral cornea ranges from 612 to 640 μm thick [21]. The cornea receives its nutrients mainly from the aqueous humor, as it is an avascular structure. Cellular components of the cornea include epithelial cells, keratocytes, and endothelial cells. Acellular components of the cornea form a matrix of collagen and glycosaminoglycans. Corneal transparency is based on uniformity of collagen fibril diameter and packing [22].

2.3 Healthy cornea parameters

UHR-OCT of the healthy cornea is important in order to recognize changes in disease states (**Figure 1**). UHR-OCT parameters of the normal tear film were first reported by Werkmeister et al. [10]. The group reported an average central tear

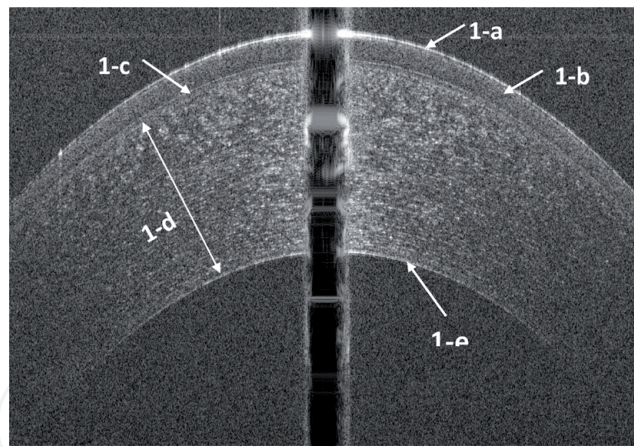


Figure 1. A prototypical cross-sectional UHR-OCT image of a healthy human cornea. Epithelium (1b), Bowman's layer (1c), stroma (1d), and endothelium/Descemet membrane complex (1e) can be distinguished. The topmost highly reflective layer in the tomogram represents the pre-corneal tear film (1-a).

film thickness of $4.79\ \mu\text{m}$ [23]. Other reported central tear film thicknesses include $3.4\ \mu\text{m}$ [24], $5.1\ \mu\text{m}$ [25] and a range of $3\text{--}8\ \mu\text{m}$ [26]. The central cornea measured $585\ \mu\text{m}$, with epithelial thicknesses of $55\ \mu\text{m}$ [10] and $55.8\ \mu\text{m}$ [25].

Data from a SD-OCT with $3.9\ \mu\text{m}$ axial resolution showed that central corneal epithelium thickness is not statistically significant between subjects less than or greater than 40 years old (48.3 and $48.8\ \mu\text{m}$, respectively) [27]. This conclusion was supported by previous studies which showed no alteration in epithelial cell density with age [28]. Epithelial thickness varied over the vertical and horizontal meridians from 42.9 to $55.2\ \mu\text{m}$ and 58.6 to $59.3\ \mu\text{m}$, respectively [29].

Bowman's layer has been reported as $18\ \mu\text{m}$ [10] and $18.7\ \mu\text{m}$ [25] thick with an uneven thickness distribution over the horizontal meridian of the cornea [25]. The central and midperiphery, nasal, temporal Bowman's layer thickness was 17.7 , 20.0 and $19.8\ \mu\text{m}$, respectively [25]. Thickness gradually increases from temporal to nasal and from inferior to superior [25].

The Endothelium/Descemet membrane complex (En/DM) is made of Descemet membrane (DM), endothelium, and retro-corneal membranes. These layers are typically indistinguishable so the thickness measured from UHR-OCT is different from that from pathology [30]. DM in healthy young subjects is seen with UHR-OCT as a single, opaque, smooth line. The same structure is a band of two smooth opaque lines surrounding a translucent space in normal elderly subjects [9]. Bizheva et al. reported UHR-OCT data from healthy subjects, and revealed the average thickness was $6.6\ \mu\text{m}$ for pre-Descemet's layer, $10.4\ \mu\text{m}$ for Descemet's membrane and $4.8\ \mu\text{m}$ for endothelium [31]. Another group published an average central Descemet's membrane thicknesses of 10 and $16\ \mu\text{m}$ in the young and elderly healthy groups, respectively [9].

2.4 Applications of UHR-OCT for corneal microlayers

Corneal imaging has been significantly improved by the improvements in speed and resolution in the current UHR-OCT. The high axial resolution of UHR-OCT systems allows precise delineation of the corneal microlayers. There are a wide variety of clinical applications of UHR-OCT for the diagnosis and management of corneal disease [12, 13, 16, 17]. In this review, we summarize the clinical applications of imaging the ocular surface and cornea based on microlayers of the cornea.

3. Corneal pathology within the tear film

3.1 Dry eye and tear evaluation

OCT assessment of the tear meniscus has been extensively studied during the last 10 years [32]. The pathophysiology of dry eye disease is characterized by instability of the pre-corneal tear film along with increased osmolarity and ocular surface inflammation and damage [33]. Anterior segment OCT imaging in patients with dry eye disease is clinically useful as it can help directly image the tear film, Meibomian glands and conjunctival folds.

Tear film imaging is inherently limited by the fact that the tear film constantly changes with blinking [1, 23, 24, 34, 35]. OCT meniscometry solves this problem by continuously measuring the tear film, using a tear meniscus to represent the total volume. This method of acquiring images is objective, non-invasive and rapid [32, 34]. However, data analysis is complex, operator-dependent and time-consuming [36]. Tear meniscus height, curvature, and cross-sectional area are widely used in clinical practice and demonstrate good diagnostic performance and correlations with other tests [32, 34].

Cui et al. reported the first visualization of the pre-corneal tear film in dry eye patients with UHR-OCT [12]. The patients were asked to blink normally and then delay each blink as long as possible. The average pre-corneal tear film significantly increased from 4.4 μm during normal blinking to 6.6 μm during delayed blinking. The lipid layer of the tear film can be directly visualized using a contrast mechanism based on sample OCT reflectance, and measures 40–80 nm [37]. The tear film also increases on UHR-OCT after the use of artificial tears and punctal occlusion [38–41].

3.2 Contact lens fitting

UHR-OCT can perform a dynamic evaluation of contact lens movement with blinking and shifting gaze [42]. Soft contact lenses usually overlap 2 mm on the bulbar conjunctiva, but can displace further and overlap 4 to 5 mm onto the bulbar conjunctiva during blinking [43]. UHR-OCT can image the location of the edge of the lens and the tear film underneath the periphery of the lens. This data can help us to understand the normal physiology of the tear film and the dry eye associated with contact lens wear.

The tear film allows contact lens wearers to maintain vision and comfort and health [44]. Lens adherence and ocular surface staining can result from a decreased tear film [43]. Both pre-lens and post-lens tear film contribute to contact lens-associated dry eye [44]. Chen et al. imaged the tear film of 22 subjects before and after contact lens wear with a 15 mm scan width and 3 μm resolution UHR-OCT. Data showed that the pre-lens tear film increased after the instillation of artificial tears, whereas the post-lens tear film remained the same [18]. Cui et al. used UHR-OCT to study soft contact lens conjunctival overlap and the post-lens tear film. They found that increased conjunctival overlap was associated with reduced post-lens tear film underneath the peripheral region of soft contact lens during lens daily wear. Contact lenses with rounded edges also had more conjunctival overlap than the lenses with angled edges [43].

4. Corneal epithelial pathology

4.1 Dry eye

Artificial tears eye drops use increased central corneal epithelial and mid-peripheral corneal thickness in dry eye patients. Epithelial thickness can be a useful

measurement when evaluating treatment response in dry eye patients, but the pattern of epithelial changes in this disease remains inconclusive [45]. The epithelium has been reported to be thinner [46–47], the same [48], and thicker [49] in dry eye patients in several conflicting studies. Central epithelial thickness in female dry eye patients was thicker than that of normal control patients by 6.5 and 6.2 μm , respectively [49]. Further cell morphology studies may be warranted to differentiate the possible explanations of increased epithelial thickness associated with dry eye. Epithelial hypertrophy or hyperplasia, edema, or increased number of cellular layers may be contributing [49]. Abou Shousha et al. demonstrated that dry eye patients had increased corneal epithelial irregularity compared to controls, quantified by corneal epithelial thickness profile variance and range. Both parameters were significantly correlated with questionnaire scores and improved after dry eye treatment [50].

4.2 Subclinical keratoconus

Xu et al. reported UHR-OCT epithelial vertical thickness profiles in the diagnosis of subclinical keratoconus. Data showed statistically significant thinning of the central corneal epithelium; 53.48 μm in normal eyes and 51.92 μm in those with subclinical keratoconus. There was no significant inferior epithelial thinning in subclinical keratoconus; 54.94 μm in normal eyes and 54.85 μm in eyes with subclinical keratoconus [51]. However, our unpublished data found that the epithelium in patients with subclinical keratoconus had localized thinning of inferior epithelium quantified with minimum thickness. We also found that the epithelium has relative superior thickening by maximum thickness and that standard deviation of epithelial thickness was increased significantly in all regions.

4.3 Keratoconus

Corneas with keratoconus show epithelial remodeling, which minimizes local topographic irregularities and improves corneal curvature [52]. Epithelial thinning precedes other corneal changes in keratoconus [53, 54], and the location of the thinnest zone of the epithelium corresponds with the steepest zone seen on Scheimpflug tomography [10]. Xu et al. reported no significant thinning of the inferior cornea in eyes with keratoconus as compared to normal eyes. However, there was significant thinning of the central epithelium; 53.48 μm in normal eyes and 46.10 μm in eyes with keratoconus [51]. Yadav et al. reported that variation in epithelial thickness across the central 3 mm was significantly larger in eyes with keratoconus. This finding was supported by Pircher et al. who wrote that “epithelial thickness, irregularity, and asymmetry seem to be the most promising diagnostic factors in terms of discriminating between keratoconic eyes and healthy eyes” [55].

4.4 Ocular surface pathology

UHR-OCT can be used for the diagnosis of ocular surface squamous neoplasia (OSSN) and detection of sub-clinical disease [16, 56, 57]. OSSN has several classical features on anterior segment OCT, including thickened, hyper-reflective epithelium with an abrupt transition from normal to abnormal epithelium [16, 57, 58]. The gold standard for diagnosis of OSSN is examination of pathology, but non-invasive methods of diagnosis are helpful as topical chemotherapy becomes increasingly utilized [16]. UHR-OCT provides high-resolution imaging with cross-sectional views; dynamic non-contact scanning modality reduces need for technical expertise compared to UBM and confocal microscopy. However, it has poor penetrance with thicker lesions and cannot reliably detect

invasion [16]. UHR-OCT is especially useful as it can non-invasively detect OSSN in the presence of other ocular surface diseases. Co-existing conditions such as mucus membrane pemphigoid or limbal stem cell deficiency make it difficult to diagnosis OSSN based on clinical exam [59].

Corneas with scarring and Salzmann's nodular degeneration have a normal-thickness epithelium overlying a dense, hyper-reflective lesion overlying Bowman's layer on UHR-OCT [16]. Epithelial hypo-reflective cysts without basement membrane thickening are seen in Meesman's dystrophy [60]. Eyes with secondary corneal amyloidosis show deposits of amyloid above Bowman's layer, and destruction of Bowman's layer as the disease progresses [61].

4.5 Physiologic changes after contact lens wear

UHR-OCT can show corneal changes after soft contact lens wear. Epithelial thickness increased by 3.5% and total corneal thickness increased by 10% after 3 hours of patching with soft contact lens wear [62]. Endothelium and Descemet membrane showed no significant change in thickness. Long-term hydrogel lens wearers have been shown to have uniform epithelial thinning [63]. Orthokeratology lenses caused the central epithelium to thin in vertical and horizontal meridians, while the mid-peripheral nasal and temporal epithelium became thicker and the superior mid-peripheral epithelium became thinner. Bowman's layer showed no change from orthokeratology lenses [64].

4.6 Monitoring corneal epithelial defects

UHR-OCT is a useful way to monitor corneal epithelial healing as it provides an objective and three-dimensional evaluation [65]. Corneal wound healing was assessed after epithelial-off corneal collagen cross-linking, and it was noted that epithelium surrounding the fluorescein stained abrasion was not fully settled to the underlying basement membrane [10, 65]. UHR-OCT can also help monitor corneal epithelial healing under a bandage contact lens and can determine the appropriate time for lens removal after pterygium excision [11].

4.7 Post-operative monitoring

UHR-OCT revealed a significant correlation between epithelial thickening and the extent of refractive correction after myopic small incision lenticule extraction. Epithelial thickening of approximately 10% was observed during the first six postoperative months and stabilized after 3 months [66]. Epithelial thickness in eyes treated with photorefractive keratectomy was significantly higher than that of normal eyes at (68.2 vs. 55.8 μm) [24]. This difference was thought to be caused by non-uniformly altered Bowman's layer [24].

Rocha et al. reported a reduction in peripheral epithelial thickness and decreased regional variation in epithelial thickness consistent with increased corneal curvature after corneal collagen crosslinking [52]. UHR-OCT of corneal wound healing after epithelial-off cross-linking correlated well with fluorescein photographs and visualized the stromal demarcation line [65]. Most of the data about the demarcation line seen in cross-linking comes from use of the SD-OCT and further research is needed [67].

Zarei-Ghanavati et al. showed that epithelium covers the Boston type I keratoprosthesis edge and seals the potential space in the interface. They proposed that failure to epithelialize this interface and lack of epithelial sealing around the keratoprosthesis edge might be associated with endophthalmitis [68].

5. Bowman's membrane pathology

5.1 Subclinical keratoconus

Vertical thickness of Bowman's layer in subclinical keratoconus was decreased inferiorly compared with normal control eyes [51]. Our group demonstrated that Bowman's layer in patients with subclinical keratoconus was significantly thinner centrally and inferiorly, and could be quantified with mean thickness, minimum thickness, Bowman's ectasia index and Bowman's ectasia index-max [69].

5.2 Keratoconus

Bowman's layer shows thinning, disintegration and breakage on pathological specimens of eyes with keratoconus (**Figure 2**). Histopathological light and electron microscopy studies of these eyes can be helpful for the diagnosis of keratoconus [70]. Interestingly, these changes happen before stromal changes [71]. About Shousha et al. demonstrated that vertical topographic thickness maps of keratoconus patients had characteristic localized relative inferior thinning of Bowman's layer. Inferior average thickness, inferior minimum thickness, Bowman's ectasia index and Bowman's ectasia index-max were all correlated with the severity of keratoconus. The inferior average thickness of Bowman's layer in eyes with keratoconus was 12 μm compared with 15 μm in normal eyes [72]. Light scatter from Bowman's layer in eyes with keratoconus was significantly higher but did not correlate with disease severity [13].

5.3 Corneal and ocular surface pathology

UHR-OCT can detect early secondary corneal amyloidosis as a dense spot in Bowman's layer [61]. Corneas with Thiel-Behnke Dystrophy have extensive deposits of hyper-reflective material in a saw-tooth pattern on the surface of Bowman's layer [60]. UHR-OCT images may become adjunct to clinical evaluation and provide an optical biopsy image in other conditions. Eyes with spheroidal degeneration show cystic structures in Bowman's layer and superficial stroma, and Salzmann's nodular degeneration has hyper-reflective material which replaces anterior stroma and Bowman's layer with thin epithelium [60] (**Figure 2**). Limbal stem cell deficiency exhibits a hyper-reflective material which replaces Bowman's layer as well as the anterior stroma, with irregular overlying epithelium (**Figure 3**).

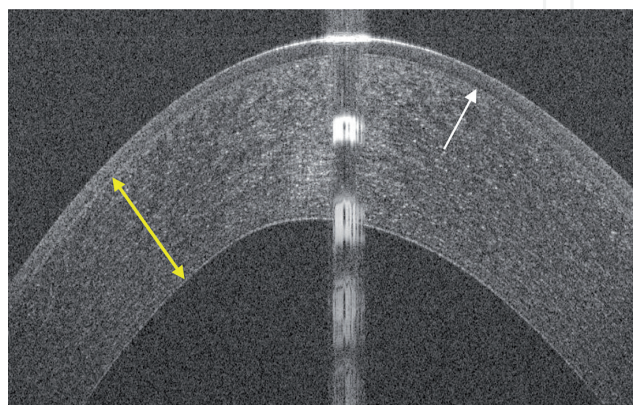


Figure 2.

A prototypical cross-sectional UHR-OCT image of a human cornea with keratoconus; focal disintegration of Bowman's layer (white arrow), focal stromal thinning (yellow arrow).

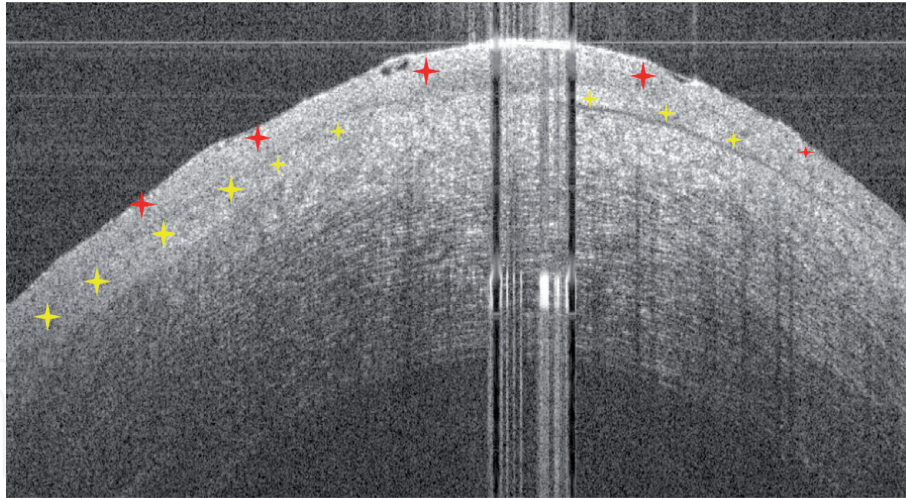


Figure 3.

A prototypical cross-sectional UHR-OCT image of a human cornea with Limbal stem cell deficiency; a hyper-reflective material (yellow stars) which replaces anterior stroma and Bowman's layer with irregular overlying epithelium (red stars).

5.4 Eyes after refractive surgery

Bowman's layer significantly decreases in eyes after photorefractive keratectomy, and was on average $14.0\ \mu\text{m}$ compared with normal eyes at $18.7\ \mu\text{m}$. There is significant variability after photorefractive keratectomy with some regions thicker than in normal eyes but most much thinner. The procedure also causes uneven epithelial thickness [24].

6. Corneal pathology within stroma

6.1 Corneal inflammatory and infectious diseases

UHR-OCT can help with the diagnosis of Acanthamoeba and herpetic keratitis. Acanthamoeba cysts show up as highly reflective dots in the stroma and radial keratoneuritis presents as thickening of the corneal nerves with ragged borders [10]. In post-herpetic keratitis corneas, UHR-OCT shows corneal thinning with areas of calcification and lipid deposition as single highly reflective scattering zones. Corneal neovascularization also appears as a hypo-reflective zone [10].

UHR-OCT is especially useful for assessment of corneal thinning in cases of impending perforation. Rodriguez et al. evaluated the use of UHR-OCT in the differentiation of inflammatory versus non-inflammatory, such as Terrien Marginal Degeneration, causes of peripheral corneal thinning. In the inflammatory group, UHR-OCT revealed a hyper-reflective subepithelial band in the area of thinning, which was not seen in Terrien marginal degeneration [73].

6.2 Stromal corneal dystrophies

UHR-OCT can evaluate the depth of deposits in stromal corneal dystrophies, which can be used to guide surgical therapy. Eyes with granular dystrophy show hyper-reflective material in the anterior stroma and clear intervening spaces. Macular dystrophy corneas show hyper-reflective stroma with areas of discrete, small hyper-reflective deposits in the subepithelial space, stroma, and Descemet's membrane [60].

6.3 Refractive surgery

UHR-OCT can be used to analyze the integrity of the corneal flap. High resolution structural characteristics of the opaque bubble layer can predict incomplete lamellar flap dissections. The opaque bubble layer can also be seen to extend anterior to the flap dissection plane up to Bowman's membrane [74]. UHR-OCT can also image progression of flap melt and epithelial ingrowth [2].

6.4 Subclinical keratoconus

Xu et al. reported that stromal vertical thickness profiles in eyes with subclinical keratoconus were thinner inferiorly compared with normal eyes [51]. Another group showed focal inferotemporal thinning, slightly more inferior than temporal. However, the degree of relative thinning was not as significant as on the epithelial pattern deviation map [75].

6.5 Keratoconus

Eyes with keratoconus had a thinner stromal thickness than normal eyes for the entire vertical meridian profile. In the keratoconus group, the thinnest central stromal thickness was 383.8 μm [51]. Sandali et al. used Fourier-domain OCT to create a reproducible classification scheme for patient with keratoconus [76]. Fuentes et al. used Fourier-domain OCT (5 mm of axial resolution) to look for risk factors for hydrops in advanced keratoconus. They revealed that features such as increased epithelial thickness, Bowman's layer hyper-reflection, and stromal thinning at the cone may be associated with increased risk [77]. UHR-OCT is also useful to identify depth of crosslinking (**Figure 4**). However, Rocha et al. demonstrated that there were no significant differences in regional stromal thickness profiles at any corneal location after corneal collagen crosslinking for eyes with either keratoconus or postoperative corneal ectasia [52].

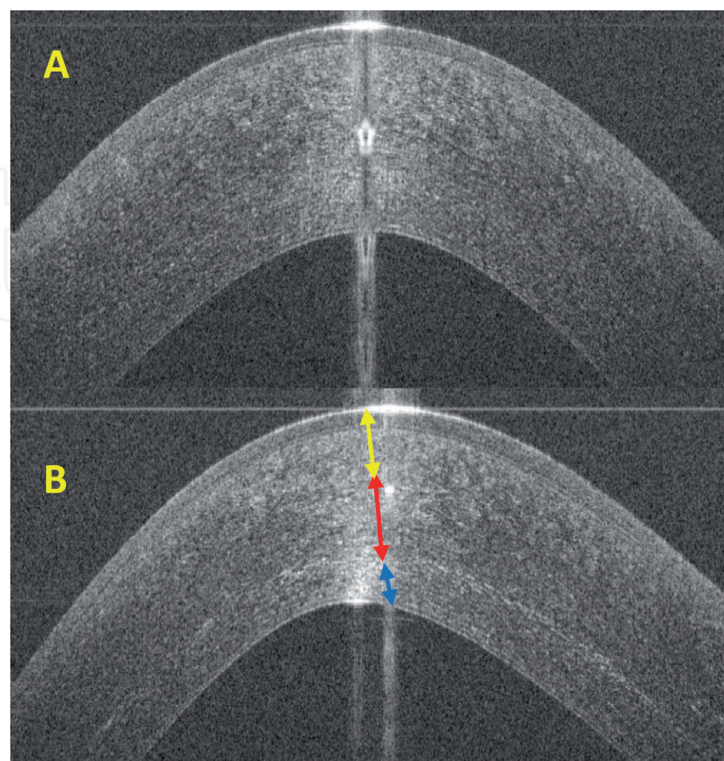


Figure 4. Prototypical cross-sectional UHR-OCT images of keratoconus before (a) and 1 month after collagen cross-linking (B); cross-linking demarcation band thickness (red arrow), depth (yellow arrow), and base (blue arrow).

7. Corneal pathology within endothelium/Descemet membrane complex (En/DM)

7.1 Fuchs' endothelial corneal dystrophy

Abou Shousha et al. published UHR-OCT characteristics of Fuchs' dystrophy patients. Descemet membrane appeared as a thickened band with two opaque lines; the anterior line was smooth while the posterior line was wavy and irregular with areas of focal thickening (**Figure 5**) [9]. Descemet membrane thickness was increased in Fuchs' dystrophy patients compared with normal subjects [9].

7.2 Detection of corneal graft rejection

Basement membrane thickening has previously been established as evidence of graft rejection in solid organs transplantation [78, 79]. Abou Shousha et al. demonstrated that thickening of the En/DM also occurs in corneal graft rejection (**Figure 6**) [80]. This study was limited by the resolution of HD-OCT as it was not possible to differentiate

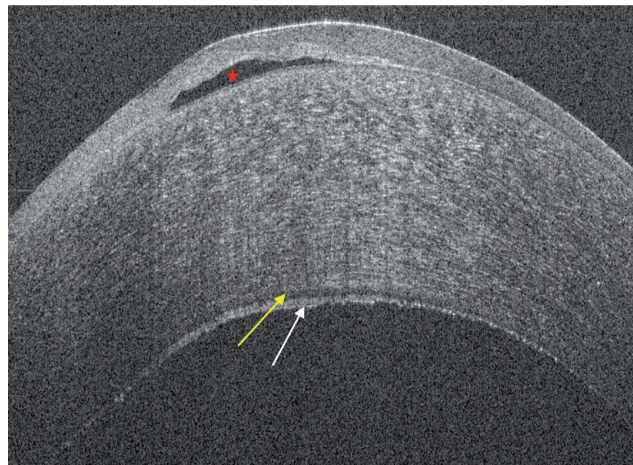


Figure 5. *A prototypical cross-sectional UHR-OCT image of a human cornea with Fuchs' endothelial dystrophy; sub-epithelial vesicle (red star), Descemet membrane appeared as a thickened band with two opaque lines; the anterior line (yellow arrow) was smooth while the posterior line (white arrow) was wavy and irregular with areas of focal thickening.*



Figure 6. *A prototypical cross-sectional UHR-OCT image of a full thickness corneal transplant with active rejection: Descemet membrane appeared as a thickened band with two hyper-reflective lines; the anterior line (yellow arrow) was smooth while the posterior line (white arrow) was wavy, broader with occasional nodular excrescences.*

between Descemet membrane, endothelium, and a potential retro-corneal membrane. Subsequent *ex vivo* data revealed that Descemet membrane is responsible for thickening of the En/DM complex in rejected corneal grafts [30].

7.3. Monitoring surgical patients

Transient corneal edema seen after phacoemulsification was caused by changes in the central corneal thickness, stroma and En/DM complex. There were no significant post-operative changes in Bowman's layer or epithelium. Pre-operative En/DM thickness may indicate the integrity of the endothelium and could be used to predict endothelial cell loss after phacoemulsification [81].

8. Corneal graft screening

Donor tissue quality is critical in the outcome of corneal transplantation [82]. Specular microscopy is the current gold standard for corneal graft screening, but only evaluates the health of the endothelium. We do not currently have an efficient method to screen for epithelial and stromal pathology such as prior refractive surgery, keratoconus or stromal opacities [82]. UHR-OCT can evaluate response to tissue processing in lamellar keratoplasty by revealing interface debris and cavitation bubbles after treatment with femtosecond laser, which may be used to correlate with post-operative outcomes [83]. Our unpublished data demonstrated the use of UHR-OCT to measure the En/DM complex thickness in donor corneas in a sterile container, and has promising results to screen grafts for early endothelial changes [84].

9. Future directions

Future developments include clinical application of the technique to screen donor corneas before transplantation. The newest generation of imaging, micro-OCT (μ OCT), uses an isotropic spatial resolution of 1–2 μ m. It can detect key cellular and subcellular components such as keratocytes, collagen fibers and corneal nerves. This new technology has the potential to improve our understanding of corneal anatomy and disease.

10. Conclusions

UHR-OCT of the anterior segment enables us to perform an optical biopsy of the tear film and all layers in the cornea in normal subjects and those with pathology. These advancements provide understanding about pathological changes in microlayers of the cornea. The main advantages of the OCT include the rapid, non-invasive, *in vivo* imaging of structures with quantitative measurements. Recent improvements in OCT technology have led to an increase in clinical and research applications. Novel developments, such as the new-generation micro-OCT and artificial intelligence, have the potential to revolutionize corneal disease diagnosis and classifications.

Conflict of interest

Vatookarn Roongpoovapatr, Jane Cook and Taher K. Eleiwa—None to declare.

Sonia H. Yoo and Mohamed Abou Shousha—.

Financial Support: This study was supported by a NEI K23 award (K23EY026118), NEI core center grant to the University of Miami (P30 EY014801), and Research to Prevent Blindness (RPB).

The funding organization had no role in the design or conduct of this research.

Conflict of Interest: United States Non-Provisional Patents (Application No. 8992023 and 61809518), and PCT/US2018/013409. Patents and PCT are owned by University of Miami and licensed to Resolve Ophthalmics, LLC. Mohamed Abou Shousha is an equity holder and sits on the Board of Directors for Resolve Ophthalmics, LLC.

Sonia Yoo is a co-inventor of intellectual property used in the study.

Author details

Vatookarn Roongpoovapatr^{1,2}, Jane C. Cook^{1*}, Taher K. Eleiwa^{1,3}, Sonia H. Yoo¹ and Mohamed Abou Shousha¹


¹ Miller School of Medicine, Bascom Palmer Eye Institute, University of Miami, Miami, FL, United States

² Department of Ophthalmology, Mettapracharak (Wat Raikhing) Hospital, Nakorn-Pathom, Thailand

³ Department of Ophthalmology, Faculty of Medicine, Benha University, Egypt

*Address all correspondence to: janecatycook@gmail.com

IntechOpen

© 2019 The Author(s). Licensee IntechOpen. This chapter is distributed under the terms of the Creative Commons Attribution License (<http://creativecommons.org/licenses/by/3.0>), which permits unrestricted use, distribution, and reproduction in any medium, provided the original work is properly cited. 

References

- [1] Ang M, Baskaran M, Werkmeister RM, et al. Anterior segment optical coherence tomography. *Progress in Retinal and Eye Research*. 2018;**66**:132-156
- [2] Wang J, Abou Shousha M, Perez VL, et al. Ultra-high resolution optical coherence tomography for imaging the anterior segment of the eye. *Ophthalmic Surgery, Lasers & Imaging*. 2011;**42** (Suppl):S15-S27
- [3] Bajwa A, Aman R, Reddy AK. A comprehensive review of diagnostic imaging technologies to evaluate the retina and the optic disk. *International Ophthalmology*. 2015;**35**:733-755
- [4] Han SB, Liu Y-C, Noriega KM, Mehta JS. Applications of anterior segment optical coherence tomography in cornea and ocular surface diseases. *Journal of Ophthalmology*. 2016:4971572
- [5] Maeda N. Optical coherence tomography for corneal diseases. *Eye & Contact Lens*. 2010;**36**:254-259
- [6] Huo T, Wang C, Zhang X, et al. Ultrahigh-speed optical coherence tomography utilizing all-optical 40 MHz swept-source. *Journal of Biomedical Optics*. 2015;**20**:030503
- [7] Kolb JP, Klein T, Kufner CL, et al. Ultra-widefield retinal MHz-OCT imaging with up to 100 degrees viewing angle. *Biomedical Optics Express*. 2015;**6**:1534-1552
- [8] Zhi Z, Qin W, Wang J, et al. 4D optical coherence tomography-based micro-angiography achieved by 1.6-MHz FDML swept source. *Optics Letters*. 2015;**40**:1779-1782
- [9] Shousha MA, Perez VL, Wang J, et al. Use of ultra-high-resolution optical coherence tomography to detect in vivo characteristics of Descemet's membrane in Fuchs' dystrophy. *Ophthalmology*. 2010;**117**:1220-1227
- [10] Werkmeister RM, Sapeta S, Schmidl D, et al. Ultrahigh-resolution OCT imaging of the human cornea. *Biomedical Optics Express*. 2017;**8**:1221-1239
- [11] Chen D, Lian Y, Li J, et al. Monitor corneal epithelial healing under bandage contact lens using ultrahigh-resolution optical coherence tomography after pterygium surgery. *Eye & Contact Lens*. 2014;**40**:175-180
- [12] Cui L, Wang J, Perez VL, et al. Visualization of the precorneal tear film using ultrahigh resolution optical coherence tomography in dry eye. *Eye & Contact Lens*. 2012;**38**:240-244
- [13] Yadav R, Kottaiyan R, Ahmad K, Yoon G. Epithelium and Bowman's layer thickness and light scatter in keratoconic cornea evaluated using ultrahigh resolution optical coherence tomography. *Journal of Biomedical Optics*. 2012;**17**(11):116010
- [14] Huang D, Swanson EA, Lin CP, et al. Optical coherence tomography. *Science*. 1991;**254**:1178-1181
- [15] Qazi Y, Aggarwal S, Hamrah P. Image-guided evaluation and monitoring of treatment response in patients with dry eye disease. *Graefe's Archive for Clinical and Experimental Ophthalmology*. 2014;**252**:857-872
- [16] Thomas BJ, Galor A, Nanji AA, et al. Ultra high-resolution anterior segment optical coherence tomography in the diagnosis and management of ocular surface squamous neoplasia. *The Ocular Surface*. 2014;**12**:46-58
- [17] Drexler W. Ultrahigh-resolution optical coherence tomography. *Journal of Biomedical Optics*. 2004;**9**:47-74

- [18] Chen Q, Wang J, Tao A, et al. Ultrahigh-resolution measurement by optical coherence tomography of dynamic tear film changes on contact lenses. *Investigative Ophthalmology & Visual Science*. 2010;**51**:1988-1993
- [19] Chen J, Lee L. Clinical applications and new developments of optical coherence tomography: An evidence-based review. *Clinical & Experimental Optometry*. 2007;**90**:317-335
- [20] Sridhar MS. Anatomy of cornea and ocular surface. *Indian Journal of Ophthalmology*. 2018;**66**:190-194
- [21] Feizi S, Jafarinasab MR, Karimian F, et al. Central and peripheral corneal thickness measurement in normal and keratoconic eyes using three corneal pachymeters. *J. Ophthalmic Vis. Res*. 2014;**9**:296-304
- [22] Meek KM, Fullwood NJ. Corneal and scleral collagens- a microscopist's perspective. *Micron*. 2001;**32**:261-272
- [23] Dua HS, Faraj LA, Said DG, et al. Human corneal anatomy redefined: A novel pre-Descemet's layer (Dua's layer). *Ophthalmology*. 2013;**120**:1778-1785
- [24] Werkmeister RM, Alex A, Kaya S, et al. Measurement of tear film thickness using ultrahigh-resolution optical coherence tomography. *Investigative Ophthalmology & Visual Science*. 2013;**54**:5578-5583
- [25] Wang J, Aquavella J, Palakuru J, et al. Relationships between central tear film thickness and tear menisci of the upper and lower eyelids. *Investigative Ophthalmology & Visual Science*. 2006;**47**:4349-4355
- [26] Schmoll T, Unterhuber A, Kolbitsch C, et al. Precise thickness measurements of Bowman's layer, epithelium, and tear film. *Optometry and Vision Science*. 2012;**89**:E795-E802
- [27] Dos Santos VA, Schmetterer L, Triggs GJ, et al. Super-resolved thickness maps of thin film phantoms and in vivo visualization of tear film lipid layer using OCT. *Biomedical Optics Express*. 2016;**7**:2650-2670
- [28] Francoz M, Karamoko I, Baudouin C, Labbé A. Ocular surface epithelial thickness evaluation with spectral-domain optical coherence tomography. *Investigative Ophthalmology & Visual Science*. 2011;**52**:9116-9123
- [29] Niederer RL, Perumal D, Sherwin T, McGhee CNJ. Age-related differences in the normal human cornea: A laser scanning in vivo confocal microscopy study. *The British Journal of Ophthalmology*. 2007;**91**:1165-1169
- [30] Du C, Wang J, Cui L, et al. Vertical and horizontal corneal epithelial thickness profiles determined by ultrahigh resolution optical coherence tomography. *Cornea*. 2012;**31**:1036-1043
- [31] Tao A, Wang J, Chen Q, et al. Topographic thickness of Bowman's layer determined by ultra-high resolution spectral domain-optical coherence tomography. *Investigative Ophthalmology & Visual Science*. 2011;**52**:3901-3907
- [32] VanDenBerg R, Diakonov VF, Bozung A, et al. Descemet membrane thickening as a sign for the diagnosis of corneal graft rejection: An ex vivo study. *Cornea*. 2017;**36**:1535-1537
- [33] Bizheva K, Haines L, Mason E, et al. In vivo imaging and morphometry of the human pre-Descemet's layer and endothelium with ultrahigh-resolution optical coherence tomography. *Investigative Ophthalmology & Visual Science*. 2016;**57**:2782-2787
- [34] Wolffsohn JS, Arita R, Chalmers R, et al. TFOS DEWS II diagnostic methodology report. *The Ocular Surface*. 2017;**15**:539-574

- [35] Craig JP, Nelson JD, Azar DT, et al. TFOS DEWS II report executive summary. *The Ocular Surface*. 2017;**15**:802-812
- [36] Wang J, Palakuru JR, Aquavella JV. Correlations among upper and lower tear menisci, noninvasive tear break-up time, and the Schirmer test. *American Journal of Ophthalmology*. 2008;**145**:795-800
- [37] Li J, Shen M, Wang J, et al. Clinical significance of tear menisci in dry eye. *Eye & Contact Lens*. 2012;**38**:183-187
- [38] Tittler EH, Bujak MC, Nguyen P, et al. Between-grader repeatability of tear meniscus measurements using Fourier-domain OCT in patients with dry eye. *Ophthalmic Surgery, Lasers & Imaging*. 2011;**42**:423-427
- [39] Schmidl D, Schmetterer L, Witkowska KJ, et al. Tear film thickness after treatment with artificial tears in patients with moderate dry eye disease. *Cornea*. 2015;**34**:421-426
- [40] Wozniak PA, Schmidl D, Bata AM, et al. Effect of different lubricant eye gels on tear film thickness as measured with ultrahigh-resolution optical coherence tomography. *Acta Ophthalmologica*. 2017;**95**:e307-e313
- [41] Kaya S, Schmidl D, Schmetterer L, et al. Effect of hyaluronic acid on tear film thickness as assessed with ultra-high resolution optical coherence tomography. *Acta Ophthalmologica*. 2015;**93**:439-443
- [42] Li M, Wang J, Shen M, et al. Effect of punctal occlusion on tear menisci in symptomatic contact lens wearers. *Cornea*. 2012;**31**:1014-1022
- [43] Cui L, Shen M, Wang MR, Wang J. Micrometer-scale contact lens movements imaged by ultrahigh-resolution optical coherence tomography. *American Journal of Ophthalmology*. 2012;**153**:275-283.e1
- [44] Cui L, Chen S, Zhou W, et al. Characterization of soft contact lens edge fitting during daily wear using ultrahigh-resolution optical coherence tomography. *Journal of Ophthalmology*. 2018;**3463595**:1-7
- [45] Wang J, Jiao S, Ruggeri M, et al. In situ visualization of tears on contact lens using ultra high resolution optical coherence tomography. *Eye & Contact Lens*. 2009;**35**:44-49
- [46] Çakır B, Doğan E, Çelik E, et al. Effects of artificial tear treatment on corneal epithelial thickness and corneal topography findings in dry eye patients. *Journal Français d'Ophtalmologie*. 2018;**41**:407-411
- [47] Erdélyi B, Kraak R, Zhivov A, et al. In vivo confocal laser scanning microscopy of the cornea in dry eye. *Graefes' Archive for Clinical and Experimental Ophthalmology*. 2007;**245**:39-44
- [48] Villani E, Galimberti D, Viola F, et al. The cornea in Sjogren's syndrome: An in vivo confocal study. *Investigative Ophthalmology & Visual Science*. 2007;**48**:2017-2022
- [49] El-Fayoumi D, Youssef MM, Khafagy MM, et al. Assessment of corneal and tear film parameters in rheumatoid arthritis patients using anterior segment spectral domain optical coherence tomography. *Ocular Immunology and Inflammation*. 2018;**26**:632-638
- [50] Tuominen ISJ, Konttinen YT, Vesaluoma MH, et al. Corneal innervation and morphology in primary Sjogren's syndrome. *Investigative Ophthalmology & Visual Science*. 2003;**44**:2545-2549
- [51] Kanellopoulos AJ, Asimellis G. In vivo 3-dimensional corneal epithelial thickness mapping as an indicator of dry eye: Preliminary clinical assessment.

American Journal of Ophthalmology. 2014;**57**:63-68.e2

[52] Xu Z, Jiang J, Yang C, et al. Value of corneal epithelial and Bowman's layer vertical thickness profiles generated by UHR-OCT for sub-clinical keratoconus diagnosis. *Scientific Reports*. 2016;**6**:31550

[53] Rocha KM, Rocha KM, Perez-Straziota CE, et al. Epithelial and stromal remodeling after corneal collagen cross-linking evaluated by spectral-domain OCT. *Journal of Refractive Surgery*. 2014;**30**:122-127

[54] Catalan S, Cadarso L, Esteves F, et al. Assessment of corneal epithelial thickness in asymmetric keratoconic eyes and normal eyes using Fourier domain optical coherence tomography. *Journal of Ophthalmology*. 2016;**5697343**:1-7

[55] Temstet C, Sandali O, Bouheraoua N, et al. Corneal epithelial thickness mapping using Fourier-domain optical coherence tomography for detection of forme fruste keratoconus. *Journal of Cataract and Refractive Surgery*. 2015;**41**:812-820

[56] Pircher N, Schwarzhans F, Holzer S, et al. Distinguishing keratoconic eyes and healthy eyes using ultrahigh-resolution optical coherence tomography-based corneal epithelium thickness mapping. *American Journal of Ophthalmology*. 2018;**189**:47-54

[57] Medina CA, Plesec T, Singh AD. Optical coherence tomography imaging of ocular and periocular tumours. *The British Journal of Ophthalmology*. 2014;**98**(Suppl 2):ii40-ii46

[58] Shousha MA, Karp CL, Perez VL, et al. Diagnosis and management of conjunctival and corneal intraepithelial neoplasia using ultra high-resolution optical coherence tomography. *Ophthalmology*. 2011;**118**:1531-1537

[59] Shousha MA, Karp CL, Canto AP, et al. Diagnosis of ocular surface lesions using ultra-high-resolution optical coherence tomography. *Ophthalmology*. 2013;**120**:883-891

[60] Ong SS, Vora GK, Gupta PK. Anterior segment imaging in ocular surface squamous neoplasia. *Journal of Ophthalmology*. 2016;**5435092**:1-12

[61] Atallah M, Joag M, Galor A, et al. Role of high resolution optical coherence tomography in diagnosing ocular surface squamous neoplasia with coexisting ocular surface diseases. *The Ocular Surface*. 2017;**15**:688-695

[62] Vajzovic LM, Karp CL, Haft P, et al. Ultra high-resolution anterior segment optical coherence tomography in the evaluation of anterior corneal dystrophies and degenerations. *Ophthalmology*. 2011;**118**:1291-1296

[63] Araki-Sasaki K, Osakabe Y, Fukuoka H, et al. Findings of secondary corneal amyloidosis with ultrahigh-resolution optical coherence tomography. *Clinical Ophthalmology*. 2014;**8**:2115-2119

[64] Hutchings N, Simpson TL, Hyun C, et al. Swelling of the human cornea revealed by high-speed, ultrahigh-resolution optical coherence tomography. *Investigative Ophthalmology & Visual Science*. 2010;**51**:4579-4584

[65] Pérez JG, Méjome JMG, Jalbert I, et al. Corneal epithelial thinning profile induced by long-term wear of hydrogel lenses. *Cornea*. 2003;**22**:304-307

[66] Lian Y, Shen M, Jiang J, et al. Vertical and horizontal thickness profiles of the corneal epithelium and Bowman's layer after orthokeratology. *Investigative Ophthalmology & Visual Science*. 2013;**54**:691-696

[67] Bata AM, Witkowska KJ, Wozniak PA, et al. Effect of a matrix therapy

agent on corneal epithelial healing after standard collagen cross-linking in patients with keratoconus: A randomized clinical trial. *JAMA Ophthalmology*. 2016;**134**:1169-1176

[68] Luft N, Ring MH, Dirisamer M, et al. Corneal epithelial remodeling induced by small incision lenticule extraction (SMILE). *Investigative Ophthalmology & Visual Science*. 2016;**57**:OCT176-OCT183

[69] Kanellopoulos AJ, Asimellis G. Epithelial remodeling after partial topography-guided normalization and high-fluence short-duration crosslinking (Athens protocol): Results up to 1 year. *Journal of Cataract and Refractive Surgery*. 2014;**40**:1597-1602

[70] Zarei-Ghanavati S, Betancurt C, Mas AM, et al. Ultra high resolution optical coherence tomography in Boston type I keratoprosthesis. *J. Ophthalmic Vis. Res.* 2015;**10**:26-32

[71] Sykakis E, Carley F, Irion L, et al. An in depth analysis of histopathological characteristics found in keratoconus. *Pathology*. 2012;**44**:234-239

[72] Tuori AJ, Virtanen I, Aine E, et al. The immunohistochemical composition of corneal basement membrane in keratoconus. *Current Eye Research*. 1997;**16**:792-801

[73] Abou Shousha M, Perez VL, Fraga Santini Canto AP, et al. The use of Bowman's layer vertical topographic thickness map in the diagnosis of keratoconus. *Ophthalmology*. 2014;**121**:988-993

[74] Rodriguez M, Yesilirmak N, Chhadva P, et al. High-resolution optical coherence tomography in the differentiation of inflammatory versus noninflammatory peripheral corneal thinning. *Cornea*. 2017;**36**:48-52

[75] Hurmeric V, Yoo SH, Fishler J, et al. In vivo structural characteristics of the femtosecond LASIK-induced opaque bubble layers with ultrahigh-resolution SD-OCT. *Ophthalmic Surgery, Lasers & Imaging*. 2010;**41**(Suppl):S109-S113

[76] Sandali O, El Sanharawi M, Temstet C, et al. Fourier-domain optical coherence tomography imaging in keratoconus: A corneal structural classification. *Ophthalmology*. 2013;**120**:2403-2412

[77] Fuentes E, Sandali O, El Sanharawi M, et al. Anatomic predictive factors of acute corneal hydrops in keratoconus. *Ophthalmology*. 2015;**122**:1653-1659

[78] Liapis G, Singh HK, Derebail VK, et al. Diagnostic significance of peritubular capillary basement membrane multilaminations in kidney allografts: Old concepts revisited. *Transplantation*. 2012;**94**:620-629

[79] Demetris AJ, Murase N, Lee RG, et al. Chronic rejection. A general overview of histopathology and pathophysiology with emphasis on liver, heart and intestinal allografts. *Annals of Transplantation*. 1997;**2**:27-44

[80] Abou Shousha M, Yoo SH, Sayed MS, et al. In vivo characteristics of corneal endothelium/Descemet membrane complex for the diagnosis of corneal graft rejection. *American Journal of Ophthalmology*. 2017;**178**:27-37

[81] Tao A, Chen Z, Shao Y, et al. Phacoemulsification induced transient swelling of corneal Descemet's endothelium complex imaged with ultra-high resolution optical coherence tomography. *PLoS One*. 2013;**8**:e80986

[82] Ghouali W, Grieve K, Bellefqih S, et al. Full-field optical coherence tomography of human donor and pathological corneas. *Current Eye Research*. 2015;**40**:526-534

[83] Brown JS, Wang D, Li X, et al.
In situ ultrahigh-resolution optical
coherence tomography characterization
of eye bank corneal tissue processed
for lamellar keratoplasty. *Cornea*.
2008;27:802-810

[84] Chen S, Liu X, Wang N, et al.
Visualizing micro-anatomical
structures of the posterior cornea with
micro-optical coherence tomography.
Scientific Reports. 2017;7:10752

IntechOpen